# Explicit 3D finite-element model of continuous nanofibre networks

*Yong Liu, Yuris Dzenis* ✉

*Nebraska Center for Materials and Nanoscience, Department of Mechanical and Materials Engineering, University of Nebraska-Lincoln, Lincoln NE 68588, USA*
✉ *E-mail: ydzenis@unl.edu*

Published in Micro & Nano Letters; Received on 16th March 2016; Accepted on 28th July 2016

An explicit three-dimensional (3D) finite-element model for dilute nanofibre networks is presented. The model takes into account 3D structure of networks by mimicking nanomanufacturing process. Realistic elasto-plastic behaviour of individual nanofibres with failure and frictional interfibre contacts are incorporated. The model is capable of predicting through failure mechanical behaviour of nanofibre networks with large fibre reorientation and fibre breaks. Comparison of simulated force–strain behaviour with experimental data showed that predicted and experimental curves exhibited similar shapes consisting of an elastic stage, a strain-hardening stage, and a softening stage, with abrupt drops coincident with fibre breaks. The numerically predicted maximum tensile force and total failure strain were of the same magnitude as experimental results. The developed explicit model can be used to study the effects of fibre diameter and mechanical properties, network density, fibre orientation distribution, and contact conditions on mechanical behaviour of nanofibre networks. Such studies can shed light on the mechanisms of complex nonlinear deformation and failure of networks and can be used for networks design and optimisation for applications.

**1. Introduction:** Continuous nanofibres are among the most promising types of advanced fibres for their unique functional properties due to nanoconfinement, extreme surface to mass ratio, and ultrahigh strength/toughness coupled with extreme flexibility [1–3]. In most applications [3–7], nanofibres are used in the form of nanofibre networks (NFNs). Mechanical behaviour of NFNs is complex and difficult to characterise fully experimentally due to multiple simultaneous nonlinear mechanisms such as intrinsic elasto-plastic properties of nanofilaments, interfibre frictional contacts, and fibre reorientation and damage during deformation. At the same time, mechanical behaviour of NFNs is fundamental to their function in most applications [8], therefore various theories and numerical models have been proposed for predicting the mechanical behaviour of fibre networks.

In the category of analytical modelling, van Wyk [9] derived a power-law pressure–volume relation for the uniaxial compression of wool with a three-dimensional (3D) random orientation. This theory was further generalised to study mechanics of fibre assemblies under general deformation, including compression, extension, and shear [11–14]. van Wyk's theory based methods idealised fibre contacts by ignoring fibre twisting and sliding at contacts. Cox [15] developed continuum micromechanics model based on representative volume element (RVE) for predicting elastic behaviour of paper. Narter *et al.* [16] extended Cox's work to 3D anisotropic fibre webs. Cox's theory incorporated the distribution and mechanical characteristics of constituent fibres, but only accounted for the average effect of individual fibres. Neither interfibre contacts nor transverse fibre deflections were considered.

Onck *et al.* [17] developed a 2D finite-element model of cross-linked semiflexible filaments to study shear strain stiffening of filamentous protein networks. Later, this model was extended to a 3D case by introducing 3D network topology [18, 19]. These models took into account explicit fibre network structure, elastic fibre stretching and bending, but interactions between fibres were simplified to rigid cross-links. For soft fibrous networks composed of naturally curved fibres, Kabla and Mahadevan [20] developed a simple microscopic model to study their nonlinear mechanics under uniaxial loading. The model incorporated fibre curvature, fibre length, and fibre bending stiffness, and the network structure was simplified as a unit cell with minimal network connectivity. Silberstein *et al.* [21] proposed a microstructurally informed continuum-level model for studying elasto-plastic behaviour of non-woven electrospun polymer mats. The non-woven mat was simplified as a double layer triangulated network structure using RVE approach. The model was computationally efficient and took into account elasto-plastic properties of filaments and fibre stretching and bending. The simplified network geometries and connectivities adopted in [20, 21], however, did not explicitly represent complex 3D network structure and interfibre contacts. Stylianopoulos *et al.* [22] employed a multiscale modelling approach to predict mechanical behaviour of electrospun polyurethane meshes. The model introduced an RVE consisting of 3D fibrillar network accounting for fibre density and orientation in an electrospun mesh at the microscale. Its two assumptions that bending forces were negligible and that fibres could rotate freely at cross-links, however, made the predictions of mesh moduli and fibre realignment less reliable. None of the above numerical models incorporated interfibre frictional contacts and/or fibre damage or analysed failure of fibrous networks, and only Silberstein *et al.*'s work [21] took into account elasto-plastic properties of filaments.

In this Letter, we propose an explicit 3D finite-element model for dilute NFNs. The model takes into account realistic elasto-plastic properties of polymer nanofibres, 3D explicit network structure, and frictional interfibre contacts. The model is used to predict tensile behaviour of NFNs with large fibre reorientation and fibre breaks through failure. The numerical predictions are compared with experimental data.

**2. Model development:** An explicit finite-element model of NFNs was developed on the basis of LS-DYNA software. Material properties of nanofibres were obtained from quasi-static uniaxial tensile tests of single nanofibres using Nano UTM experimental system (see [2] for experimental details). For electrospun single nanofibre with diameter $D = 600$ nm manufactured using 10% polyacrylonitrile (PAN) solution, the typical engineering stress–engineering strain curve is shown in Fig. 1. It can be seen that single nanofibre behaved as an elasto-plastic material. Elasto-plastic material model was therefore used for modelling nanofibres in the network. The model incorporated elasto-plastic characteristics such as Young's modulus, yield strength, tangent

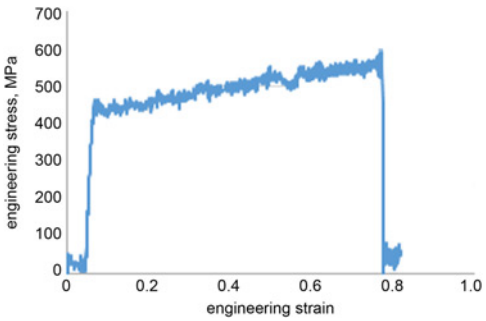


**Fig. 1** *Engineering stress–engineering strain curve from UTM tensile test for single PAN nanofibre (D = 600 nm)*

**Table 1** Key parameters of elasto-plastic material model for PAN nanofibre

| Young's modulus, GPa | Yield stress, MPa | Tangent modulus, MPa | Strain at failure |
|---|---|---|---|
| 20.77 | 463.07 | 185.30 | 0.726 |

modulus, and strain at failure. Key parameters of the material model extracted from the experimental data are listed in Table 1.

A 3D beam element was chosen for modelling nanofibres in NFNs to account for nanofibre stretching and bending. Computationally efficient and robust Hughes–Liu element with circular cross-section matching nanofibre diameter and cross-sectional integration was selected.

An automated contact detection algorithm was utilised to detect and model interfibre contacts. This algorithm generated contact forces, which resisted fibre penetration and defined fibre interactions using penalty method. General contact interactions are typically defined by specifying the external surfaces of the beam elements as contact surfaces. Sliding between fibres at the contact points is controlled by friction. The frictional coefficient $\mu_c$ is assumed to be dependent on the relative velocity of the surfaces in contact

$$\mu_c = \mathrm{FD} + (\mathrm{FS} - \mathrm{FD})\mathrm{e}^{-\mathrm{DC}\cdot|v_{\mathrm{rel}}|} \quad (1)$$

where FS is the static friction coefficient, FD is the dynamic friction coefficient, DC is the exponential decay factor, and $v_{\mathrm{rel}}$ is the relative velocity of the surfaces in contact. To the best of our knowledge, to date no research has been performed to reveal the frictional properties of nanofibres. In this Letter, friction coefficients were assumed to be FS = 1.0, FD = 0.7 × FS = 0.7 and the exponential decay factor was set to a large value, DC = 100, to ignore the unknown dependence on the relative velocity of the surfaces in contact.

The 3D structural model of a dilute NFN was developed by mimicking nanomanufacturing process. First, planar positions ($x$–$z$) of nanofibres randomly distributed in a 100 µm × 100 µm unit cell were generated by a customised MATLAB program. Different vertical positions ($y$) were assigned to each fibre so that the fibres were initially located in parallel planes. Geometric information of fibre positions was then imported to LS-DYNA. The material model, element formulation, and contact definition discussed earlier were applied in order to generate the finite-element model before the contact initialisation, as illustrated in Fig. 2. A finite-element simulation was then run and all fibres were pulled down to the lowest plane one by one by applying displacement boundary conditions at the ends of the fibres. This procedure mimicked natural interaction of nanofibres during their deposition onto substrate from

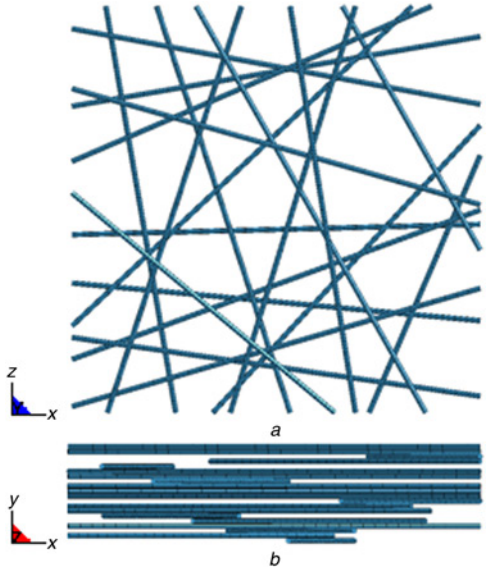


**Fig. 2** *Three-dimensional structural model of NFN before contact initialisation*
*a* Planar view ($x$–$z$)
*b* Vertical view ($x$–$y$)

the electrospun cloud [3] as well as modelled mechanical gripping of the network in mechanical tests. Natural contacts between fibres and the entangled network structure were thus initialised, as illustrated in Fig. 3.

Only the geometric information (i.e. nodes and elements positions) of the initialised model (Fig. 3) was exported for further mechanical modelling. The residual stress and strain developed in the contact initialisation process were ignored. With the exported geometric information, a rigid square frame was built around the NFN and the ends of nanofibres were fixed to the frame. Same material model, element formulation, and contact definition were then reapplied to the NFN model. The frame was cut at the centre. The left part of the frame was clamped and all degrees of freedom (DOFs) were constrained. Displacement boundary conditions were applied on the right part of the frame in $x$-direction while all other DOFs were constrained. In such way, the uniaxial tensile

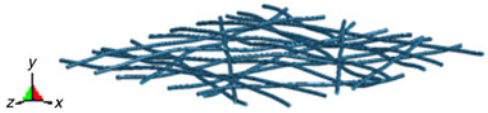


**Fig. 3** *Initialised 3D structural model of NFN*

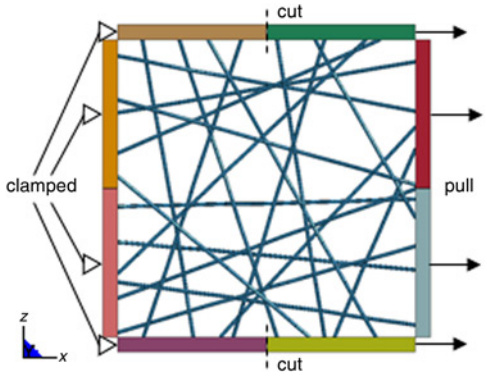


**Fig. 4** *Uniaxial tensile test model for NFN*




doi: 10.1049/mnl.2016.0147

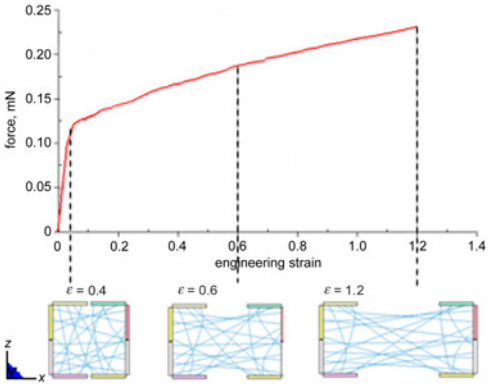


**Fig. 5** *Force–engineering strain curve and associated NFN structure evolution from tensile test simulation of NFN without fibre breaks*

test of NFN could be simulated to predict its tensile behaviour, as shown in Fig. 4.

**3. Results and discussions:** Two cases were studied with the 3D explicit finite-element model developed in the previous section. In the first case, fibre breaks were not taken into account by ignoring the parameter of strain at failure in the material model, for the purpose of observing large fibre reorientation during deformation. Simulated force–engineering strain curve and associated NFN microstructure evolution as a function of strain are shown in Fig. 5. It can be seen that the dilute NFN without fibre breaks under tensile load behaved like elasto-plastic material. At engineering strain $\varepsilon = 0.04$ the NFN effectively yielded and after that the force–strain curve went into strain-hardening stage. By tracking the NFN deformation at $\varepsilon = 0.6$ and $\varepsilon = 1.2$, large fibre reorientation was observed (Fig. 5).

In the second case, fibre breaks were incorporated by setting material model parameters according to Table 1, and more realistic simulation results were obtained. Simulated force–engineering strain curve and associated NFN microstructure evolution as a function of strain are shown in Fig. 6.

Similar to the results from the first case, the NFN effectively yielded at $\varepsilon = 0.04$ and after that the force continued increasing in a strain-hardening stage. At $\varepsilon = 0.50$, the force reached the maximum value and after that the force–strain curve went into a softening stage, in which the force decreased toward the total failure point. At total failure strain (i.e. the engineering strain beyond which the NFN can no longer carry load) $\varepsilon = 1.20$, the force decreased to 0. It can be observed that the force strain curve exhibited abrupt drops during the softening stage. By tracking associated NFN structural changes it was found that each of the drops

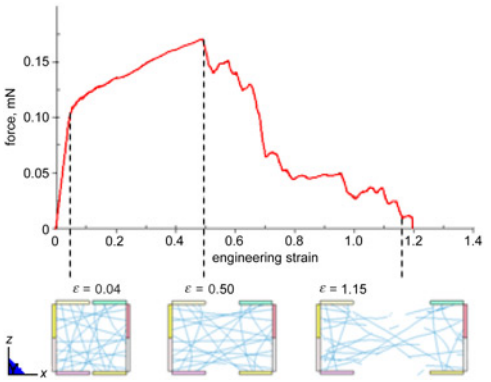


**Fig. 6** *Force–engineering strain curve and associated NFN structure evolution from tensile test simulation of NFN with fibre breaks*

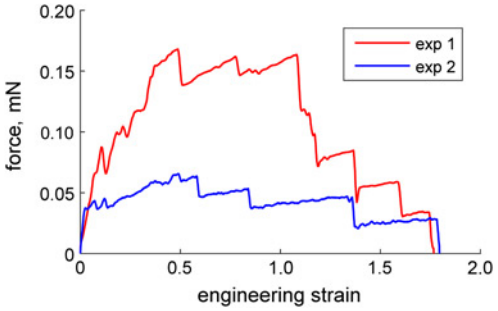


**Fig. 7** *Force–engineering strain curves from UTM tensile tests for dilute PAN NFNs*

was coincident with some fibre breaks. For example, at $\varepsilon = 0.50$ there were 2 fibre breaks and at $\varepsilon = 1.15$ there were 15 fibre beaks accumulated (see Fig. 6).

An experimental study of tensile behaviour of dilute NFNs was performed in order to qualitatively compare numerical results and experimental data. Samples of dilute NFNs were manufactured by electrospinning 10% PAN solution. Quasi-static uniaxial tensile tests for the samples were performed using Nano UTM system. Force–engineering strain curves from the tensile tests for two samples of dilute NFNs are shown in Fig. 7, from which it can be seen that the curves are not identical. This is due to structural randomness of NFNs resulting from randomness of the electrospinning process and is mainly due to randomness in fibre orientations, mechanical properties, and areal density distribution.

Similarly, in our finite-element model the distribution of fibre orientation could also cause structural randomness. In order to test this, four additional models were developed and tested using the protocol described above. All characteristics of the models were the same except the fibre orientations, which were randomly generated for each model. Simulated force–strain curves are compared in

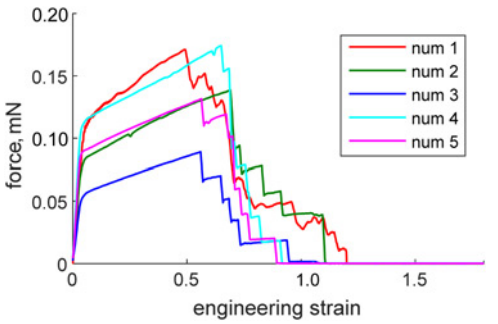


**Fig. 8** *Force–engineering strain curves from tensile test simulations for dilute NFNs with randomly generated fibre orientation distributions*

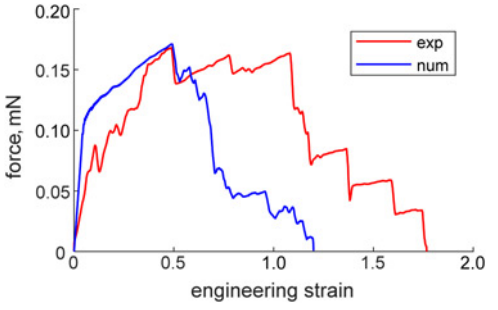


**Fig. 9** *Force–engineering strain curves from experimental and numerical tensile tests for dilute NFNs*

**Table 2** Mean values of maximum force and total failure strain from experimental and numerical tensile tests for dilute NFNs

| | Maximum force, mN | Total failure strain |
|---|---|---|
| experimental | 0.117 | 1.78 |
| numerical | 0.141 | 1.04 |

Fig. 8, from which it can be seen that the structural randomness in models would also cause randomness in the simulation results.

One curve from experimental results (Fig. 7: 'exp 1') and one from numerical simulations (Fig. 8: 'num 1') are compared in Fig. 9. It can be seen that numerical and experimental load–strain curves show qualitatively similar shapes and similar patterns of drops which are coincident with fibre breaks during NFN deformation through failure. Mean values of the maximum force and the total failure strain deduced from numerical and experimental data are compared in Table 2, from which it can be seen that in both cases the values have the same order of magnitude. In conclusion, the developed explicit 3D model is capable of capturing the pattern of nonlinear tensile behaviour of dilute NFNs through failure.

**4. Conclusions:** An explicit 3D finite-element model for dilute networks of continuous nanofibres was developed. The model utilised elasto-plastic material model and automated contact detection algorithm to incorporate realistic properties of polymer nanofibres with failure and frictional contacts between fibres. The geometric model was built by mimicking nanomanufacturing process to replicate the entangled structure of NFNs. The model was capable of predicting tensile behaviour of dilute NFNs with large fibre reorientation and fibre breaks. Numerical results were qualitatively compared with experimental data. It was found that numerical and experimental force–engineering strain curves shared similar patterns of drops which were coincident with fibre breaks, and the numerically predicted and experimental maximum force and total failure strain were of the same order of magnitude.

The developed model can be extended for studying NFN behaviour through failure under other, more general loads by applying different boundary conditions during simulations. The explicit nature of the model enables quantitative tracking of nanofibre damage and fibre reorientation accumulations in NFNs, which will be valuable in future studies of nonlinear mechanisms of NFN deformation and failure. NFN structural characteristics such as fibre density, initial fibre orientation distribution, contact conditions, and fibre diameter are controllable in the model, which enables future parametric studies of the effects of these characteristics on NFN mechanical behaviour.

**5. Acknowledgments:** This research was supported in part by the grants from NSF (DMR-1310534, CMMI-1463636), NIH (1R01HL125736-01), and ONR (N000141410663). The authors thank Cheng Ren for help with NFN experiments.

## 6 References

[1] Li D., Xia Y.N.: 'Electrospinning of nanofibers: reinventing the wheel?', *Adv. Mater.*, 2004, **16**, (14), pp. 1151–1170
[2] Papkov D., Zou Y., Andalib M.N., *ET AL.*: 'Simultaneously strong and tough ultrafine continuous nanofibers', *ACS Nano*, 2013, **7**, (4), pp. 3324–3331
[3] Dzenis Y.: 'Spinning continuous fibers for nanotechnology', *Science*, 2004, **304**, pp. 1917–1919
[4] Dzenis Y.A., Reneker D.H.: 'Delamination resistant composites prepared by small diameter fiber reinforcement at ply interfaces'. US Patent, 2001, No. 626533
[5] Leung W., Hung C.H., Yuen P.T.: 'Experimental investigation on continuous filtration of sub-micron aerosol by filter composed of dual-layers including a nanofiber layer', *Aerosol Sci. Technol.*, 2009, **43**, (12), pp. 1174–1183
[6] Venugopal J., Low S., Choon A.T., *ET AL.*: 'Interaction of cells and nanofiber scaffolds in tissue engineering', *J. Biomed. Mater. Res. B, Appl. Biomater.*, 2008, **84**, (1), pp. 34–48
[7] Jo S.M., Song M.Y., Ahn Y.R., *ET AL.*: 'Nanofibril formation of electrospun $TiO_2$ fibers and its application to dye-sensitized solar cells', *J. Macromol. Sci., Pure Appl. Chem.*, 2005, **42 A**, (11), pp. 1529–1540
[8] Wu X., Dzenis Y.: 'Elasticity of planar nanofiber networks', *J. Appl. Phys.*, 2005, **98**, 093501, pp. 1–9
[9] van Wyk C.M.: 'Note on the compressibility of wool', *J. Textile Inst.*, 1946, **37**, (12), pp. 285–292
[10] Komori T., Makishima K.: 'Number of fiber-to-fiber contacts in general fiber assemblies', *Tex. Res. J.*, 1977, **47**, (1), pp. 13–17
[11] Komori T., Itoh M.: 'Theory of the general deformation of fiber assemblies', *Tex. Res. J.*, 1991, **61**, (10), pp. 588–594
[12] Komori T., Itoh M.: 'A modified theory of fiber contact in general fiber assemblies', *Tex. Res. J.*, 1994, **64**, (9), pp. 519–528
[13] Pan N.: 'Modified analysis of the microstructural characteristics of general fiber assemblies', *Tex. Res. J.*, 1993, **63**, (6), pp. 336–345
[14] Pan N., Chen J., Seo M., *ET AL.*: 'Micromechanics of a planar hybrid fibrous network', *Tex. Res. J.*, 1997, **67**, (12), pp. 907–925
[15] Cox H.L.: 'Elasticity and strength of paper and other fibrous materials', *Br. J. Appl. Phys.*, 1952, **3**, (3), pp. 72–79
[16] Narter M.A., Batra K., Buchanan R.: 'Micromechanics of three-dimensional fibrewebs: constitutive equations', *Proc. R. Soc. Lond. A*, 1999, **455**, (1989), pp. 3543–3563
[17] Onck P.R., Koeman T., Van Dillen T., *ET AL.*: 'Alternative explanation of stiffening in cross-linked semiflexible networks', *Phys. Rev. Lett.*, 2005, **95**, (17), p. 178102
[18] Huisman E.M., Van Dillen T., Onck P.R., *ET AL.*: 'Three-dimensional cross-linked F-actin networks: relation between network architecture and mechanical behavior', *Phys. Rev. Lett.*, 2007, **99**, (20), p. 208103
[19] Zagar G., Onck P.R., Van Der Giessen E.: 'Elasticity of rigidly cross-linked networks of a thermal filaments', *Macromolecules*, 2011, **44**, (17), pp. 7026–7033
[20] Kabla A., Mahadevan L.: 'Nonlinear mechanics of soft fibre networks', *R. Soc. Interface*, 2007, **4**, (12), pp. 99–106
[21] Silberstein M.N., Pai C.L., Rutledge G.C., *ET AL.*: 'Elastic–plastic behavior of non-woven fibrous mats', *J. Mech. Phys. Solids*, 2012, **60**, (2), pp. 295–318
[22] Stylianopoulos T., Bashur C.A., Goldstein A.S., *ET AL.*: 'Computational predictions of the tensile properties of electrospun fiber meshes: effect of fiber diameter and fiber orientation', *J. Mech. Behav. Biomed. Mater.*, 2008, **1**, (4), pp. 326–335




doi: 10.1049/mnl.2016.0147